Hindawi
Journal of Mathematics
Volume 2022, Article ID 6378721, 12 pages
https://doi.org/10.1155/2022/6378721

Research Article

Computational Insights of Bioconvective Third Grade Nanofluid Flow past a Riga Plate with Triple Stratification and Swimming Microorganisms

Safak Kayikci

Department of Computer Engineering, Bolu Abant Izzet Baysal University, Bolu, Turkey

Correspondence should be addressed to Safak Kayikci; safak.kayikci@ibu.edu.tr

Received 14 June 2022; Revised 14 July 2022; Accepted 16 July 2022; Published 31 August 2022

Academic Editor: Arzu Akbulut

The goal of this study is to examine the heat-mass effects of a third grade nanofluid flow through a triply stratified medium containing nanoparticles and gyrostatic microorganisms swimming in the flow. The heat and mass fluxes are considered as a non-Fourier model. The governing models are constructed as a partial differential system. Using correct transformations, these systems are converted to an ordinary differential model. Ordinary systems are solved using convergent series solutions. The effects of physical parameters for fluid velocity, fluid temperature, nanoparticle volume percentage, motile microbe density, skin friction coefficients, local Nusselt number, and local Sherwood number are all illustrated in detail. When the values of the bioconvection Lewis number increase, the entropy rate also rises. The porosity parameter and modified Hartmann number show the opposite behaviour in the velocity profile.

1. Introduction

Researchers are interested in learning more about how to increase heat transmission because it is so important in design and business. Thermal transfer of convectional liquids such as ethylene glycol, water, and oil can be used in a variety of mechanical assemblies, electrical devices, and heat dissipates. Despite this, the thermal conductivity of these base fluids is weak. To counter this flaw, experts from several sectors are attempting to improve the heat conductivity of newly cited fluids by incorporating a unique type of nanosized particle into a new fluid known as "nanofluid," see Choi [1]. Nanofluid flow on a flat surface was examined by Khan and Pop [2]. They see that the mass transfer gradient reduces for enhancing the thermophoresis parameter. Barnoon and Toghraie [3] analyze the impact of a non-Newtonian nanofluid on aporous medium. Natural convective flow of nanofluid past a heated porous plate was demonstrated by Ghalambaz et al. [4], and they concluded that the fluid velocity creases when increasing the thermophoresis parameter. Aziz and Khan [5] demonstrated the characteristics of natural convective flow of nanofluids over a plate. They identified that heat transfer reduced by the impact of Brownian motion parameter. The nanofluid flow over a thin needle was addressed by Ahmad et al. [6]. They proved that the Brownian motion parameter leads to suppressing the nanofluid concentration. Prasannakumara et al. [7] addressed the consequences of multiple slips of MHD Jeffery nanofluid past a surface. They detected that the thermal boundary layer thickness thickens when enriching the thermophoresis parameter.

The bioconvection phenomenon is a fluid dynamic mechanism that occurs in macroscopic convective fluid flow generated by a fluid density gradient established by collective swimming of microorganisms. Because of their motility, these bacteria are classified as chemotactic, oxytactic, or gyrotactic. Near the top of the fluid layer, these self-propelled motile bacteria clump together, forming a dense upper surface that is unstable or unstabilized. Bioconvection is used in a variety of industrial applications, including microbial improved oil recovery, sustainable fuel cell technologies, water treatment facilities, polymer synthesis,

and so on. The 2D radiative flow of tangent hyperbolic nanofluid past a Riga plate with gyrotactic microorganisms was disclosed by Waqas et al. [8]. They noted that the density of motile microorganisms decays when enriching the bioconvection Lewis number. Uddin et al. [9] portrayed the consequences of Stefan blowing of bioconvective flow of nanofluid past a porous medium. They see that the density of motile microorganisms enriches when strengthening the wall suction parameter. MHD flow of cross nanofluids with gyrotactic motile microorganisms past wedge was scrutinized by Alshomrani et al. [10]. They noted that the motile microorganisms suppress when escalating the Peclet number. Muhammad et al. [11] developed the mathematical model for the unsteady MHD flow of Carreau nanofluids with bioconvection. They detected that the density of local motile number depresses when enhancing the Peclet parameter.

Due to its numerous industrial and engineering uses, such as cooling nuclear reactors, power generation, cooling of electronic equipment, energy production, and many others, the process of heat transfer has gotten a lot of attention from modern scholars. Fourier [12] was the first to present the heat transfer law. However, this law has the disadvantage of producing a parabolic energy equation. To address this flaw, Cattaneo [13] rewrote the Fourier equation by including the relaxation time heat flux component. In addition, Christov [14] tweaked the Cattaneo model by incorporating thermal relaxation time and used the Oldroyd upper convective model. The heat transport analysis of 2D flow cross nanofluid Cattaneo–Christov theory was investigated by Salahuddin et al. [15], and they proved that concentration relaxation leads to downfall of the nanofluid concentration. Farooq et al. [16] examined the impact of MHD flow of radiative nanofluids with Cattaneo–Christov theory. They revealed that the fluid temperature diminishes when raising the thermal relaxation parameter. Thermally radiative flow of hybrid nanoliquids with Cattaneo–Christov heat flux theory was implemented by Waqas et al. [17].

Despite the fact that nanofluids have been widely investigated, the third grade nanofluid flow over a stretching sheet with entropy optimization was examined by Loganathan et al. [18]. This study is extended with the effects of including the mixed convective flow of third grade nanofluids over a Riga plate with triple stratification and swimming microorganisms. The thermal radiative flow of third grade nanofluids containing microorganisms owing to the movement of the Riga plate is shown in this study to achieve this goal.

(i) The modified Fourier's law is used to frame energy and nanoparticle concentration equations

(ii) The homotopy analysis method is used to compute the non-linear equations analytically

(iii) The results of the simulations might have unique implications in the fields of thermal processes, heat transfer industry, energy systems, nuclear systems, and so on

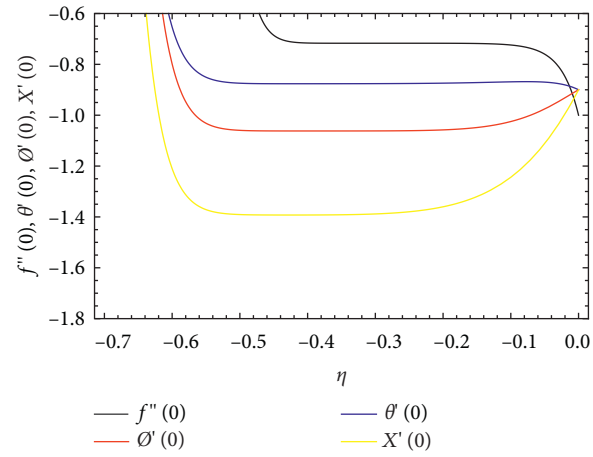

Figure 1: h-curves for $(h_f, h_\theta, h_\phi, \text{and } h_\chi)$.

2. Problem Development

For an incompressible fluid model with body forces, the continuity and motion equations are

$$\begin{aligned} \operatorname{div} v^* &= 0, \\ \rho \frac{\mathrm{d}v}{\mathrm{d}t} &= \operatorname{div} T + \rho b + J + B, \end{aligned} \tag{1}$$

where ρ is the "fluid density," v^* is the "velocity field," b is the "body forces," J is the "electric current," and T is the "third–grade incompressible fluids Cauchy stress tensor" [19].

$$\begin{aligned} T = &-pI + \mu H_1 + A_1^* H_2 + A_2^* H_1^2 + \gamma_1 H_3 \\ &+ \gamma_2 \left(H_1, H_2 + H_2 H_1\right) + \gamma_3 \left(tr H_1^2\right) H_1, \end{aligned} \tag{2}$$

where $\mu, (H_1, H_2, H_3)$ and A_1^*, γ_i –"viscosity coefficient", "kinematics tensors" and "material modulis"

$$\begin{aligned} H_1 &= L + (L)^T, \\ H_n &= \frac{\mathrm{d}}{\mathrm{d}t} H_{n-1} + H_{n-1} L + (L)^T H_{n-1}, \quad n = 2, 3, \\ L &= \nabla v^*, \end{aligned} \tag{3}$$

$\mathrm{d}/\mathrm{d}t$ is expressed as the material time derivative

$$\frac{\mathrm{d}(\,)}{\mathrm{d}t} = \frac{\partial(\,)}{\partial t} + v^* \cdot \nabla(\,). \tag{4}$$

The relationship between the Clausius–Duhem inequality and the thermodynamically compatible fluid is described by Fosdick and Rajagopal. [20].

$$\begin{aligned} &\mu \geq 0, \\ &A_1^* \geq 0, \\ &\gamma_1 = \gamma_2 = 0, \\ &\gamma_3 \geq 0, \\ &\left|A_1^* + A_2^*\right| \leq 2\sqrt{6\mu\gamma_3}, \\ &T = -pI + \mu H_1 + A_1^* H_2 + A_2^* H_1^2 + \gamma_3 \left(tr H_1^2\right) H_1. \end{aligned} \tag{5}$$

Pakdemirli [21] took into consideration the Boussinesq and normal boundary layer approximations.

The representation of steady flow of third grade nanofluids containing motile microorganisms is assumed. The surface is linearly stretched via velocity $u_w = ax$, in positive x direction in its own path. Moreover, the flow is considered along the sheet while v is perpendicular, and B_0 magnetic field is taken vertical to the flow direction. The wall temperature T_w, wall concentration C_w, and motile microorganisms' wall concentration N_w are defined. Figure 1 portrays the flow geometry of the problem. The governing equations are extended from Loganathan et al. [18] as follows:

$$\frac{\partial u}{\partial x} + \frac{\partial v}{\partial y} = 0,$$

$$u\frac{\partial u}{\partial x} + v\frac{\partial u}{\partial y} = \nu\frac{\partial^2 u}{\partial y^2} + \frac{A_1^*}{\rho}\left(u\frac{\partial^3 u}{\partial y^2 \partial x} + v\frac{\partial^3 u}{\partial y^3} + \frac{\partial u}{\partial x}\frac{\partial^2 u}{\partial y^2} + 3\frac{\partial u}{\partial y}\frac{\partial^2 u}{\partial x \partial y}\right) + 2\frac{A_2^*}{\rho}\frac{\partial u}{\partial y}\frac{\partial^2 u}{\partial x \partial y}$$

$$+ 6\frac{\beta_1^*}{\rho}\left(\frac{\partial u}{\partial y}\right)^2\frac{\partial^2 u}{\partial y^2} - \frac{\nu}{k_p}u - \frac{C_b}{x\sqrt{k_p}}u^2 + \frac{1}{\rho_f}(1 - C_\infty)\rho_f \beta g (T - T_\infty)$$

$$-\left(\rho_p - \rho_f\right)g(C - C_\infty) - (N - N_\infty)g\gamma\left(\rho_m - \rho_f\right) + \frac{\pi J_0 M_0}{8\rho}\exp\left(-\frac{\pi}{a_1}y\right)$$

$$\cdot u\frac{\partial T}{\partial x} + v\frac{\partial T}{\partial y} + \lambda_T\left(u^2\frac{\partial^2 T}{\partial x^2} + v^2\frac{\partial^2 T}{\partial y^2} + \left(u\frac{\partial u}{\partial x}\frac{\partial T}{\partial x} + v\frac{\partial u}{\partial y}\frac{\partial T}{\partial x}\right) + 2uv\frac{\partial T^2}{\partial x \partial y}\right) \tag{6}$$

$$+\left(u\frac{\partial v}{\partial x}\frac{\partial T}{\partial y} + v\frac{\partial v}{\partial y}\frac{\partial T}{\partial y}\right) = \frac{k}{\rho c_p}\frac{\partial^2 T}{\partial y^2} - \frac{1}{\rho c_p}\frac{16\sigma^*}{3k^*}\frac{\partial}{\partial y}\left(T^3\frac{\partial T}{\partial y}\right) + \frac{Q_0}{\rho c_p}(T - T_\infty) + \tau\left[D_B\frac{\partial C}{\partial y}\frac{\partial T}{\partial y} + \frac{D_T}{T_\infty}\left(\frac{\partial T}{\partial y}\right)^2\right],$$

$$u\frac{\partial C}{\partial x} + v\frac{\partial C}{\partial y} = D_B\frac{\partial^2 C}{\partial y^2} + \frac{D_T}{T_\infty}\frac{\partial^2 T}{\partial y^2} + \lambda_C\left(u^2\frac{\partial^2 C}{\partial x^2} + v^2\frac{\partial^2 C}{\partial y^2} + \left(u\frac{\partial u}{\partial x}\frac{\partial C}{\partial x} + v\frac{\partial u}{\partial y}\frac{\partial C}{\partial x}\right) + 2uv\frac{\partial C^2}{\partial x \partial y}\right)$$

$$+\left(u\frac{\partial v}{\partial x}\frac{\partial C}{\partial y} + v\frac{\partial v}{\partial y}\frac{\partial C}{\partial y}\right) - k_c(C - C_\infty),$$

$$u\frac{\partial N}{\partial x} + v\frac{\partial N}{\partial y} - D_m\left(\frac{\partial^2 N}{\partial y^2}\right) = -\frac{bW_c}{(C_W - C_\infty)}\left[\frac{\partial}{\partial y}\left(N\frac{\partial C}{\partial y}\right)\right].$$

With the boundary points

$$\begin{aligned}
&u = u_w = ax,\\
&v = 0,\\
&T = T_w = T_0 + b_1 x,\\
&C = C_W = C_0 + d_1 x,\\
&N = N_w = N_0 + e_1 x \text{ at } y = 0,\\
&\quad u \longrightarrow 0,\\
&T = T_\infty = T_0 + b_2 x,\\
&C = C_\infty\\
&N = N_\infty = N_0 + e_2 x \text{ as } y \longrightarrow \infty.
\end{aligned} \tag{7}$$

Here, b_1, b_2, d_1, d_2, e_1, and e_2 are the dimensional constants, and T_0 and C_0 are the "reference temperature and concentrations," respectively. u and v are the "velocity components" in x and y directions, ρ is the "fluid density," υ is the "fluid kinematics viscosity," k_p is the "permeability of the porous medium," C_b is the "drag coefficient," J_0 is the "current density applied to the electrodes," M_0 is the "magnetic property of the permanent magnets," a_1 is the "magnets positioned in the interval separating the electrodes," σ^* is the "Stefen-Boltzmann constant," Cp is the "specific heat capacity of the fluid," and k is the "thermal conductivity."

Transformations are declared as follows:

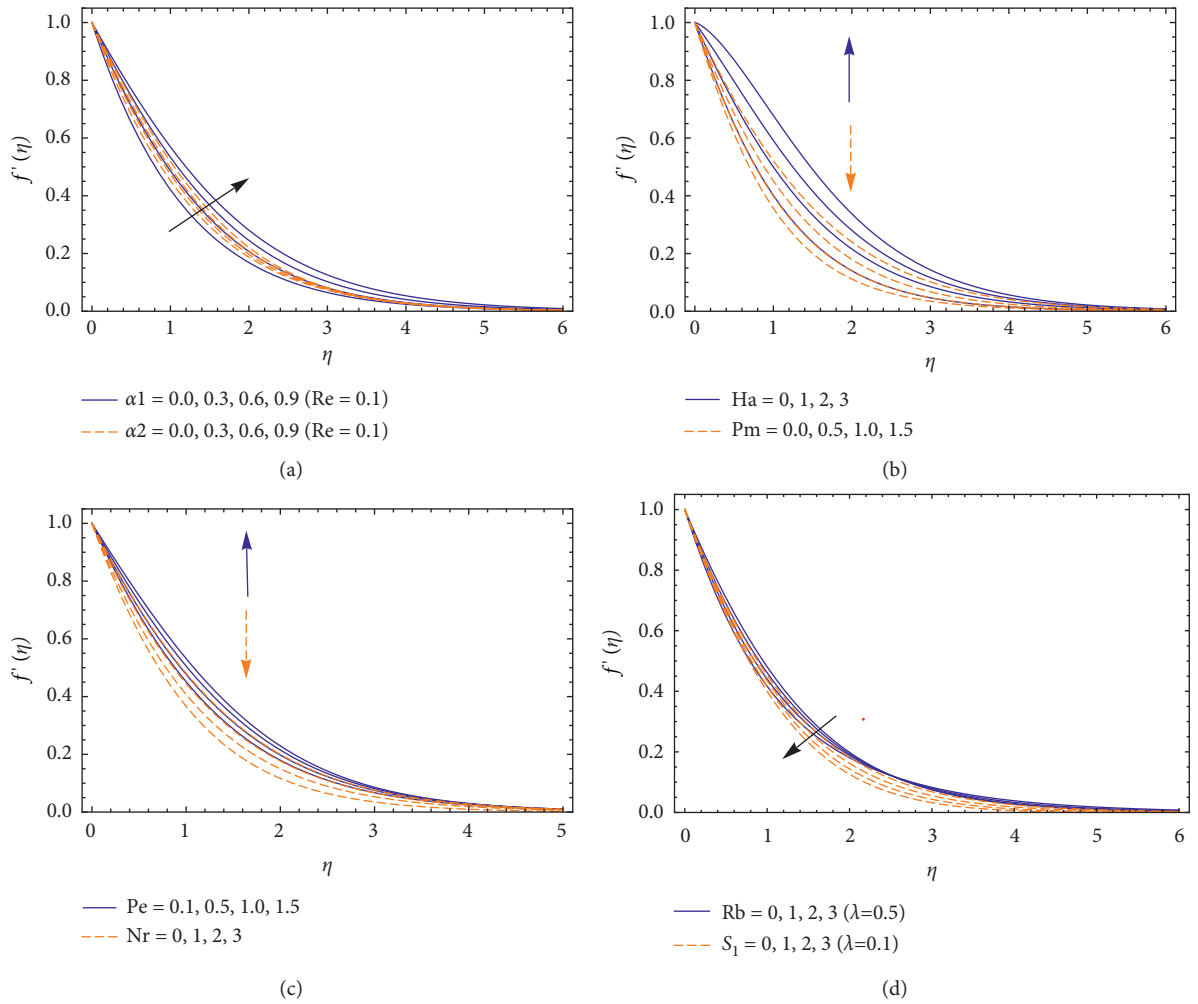

Figure 2: Velocity profile for different values of $\alpha_1, \alpha_2, Ha, P_m, Pe, Nr, Rb$, and S_1.

$$\eta = y\left(\frac{a}{\nu}\right)^{1/2},$$
$$\psi = (a\nu)^{1/2} f(\eta),$$
$$u = \frac{\partial \psi}{\partial y},$$
$$v = -\frac{\partial \psi}{\partial x},$$
$$u = u_w f'(\eta), \tag{8}$$
$$v = -(u_w)^{1/2} f(\eta),$$
$$\theta = \frac{T - T_\infty}{T_w - T_0},$$
$$\phi(\eta) = \frac{C - C_\infty}{C_w - C_0},$$
$$\chi(\eta) = \frac{N - N_\infty}{N_w - N_0}.$$

The nonlinear governing equations are

$$f''' + ff'' - f'^2 + \alpha_1\left(2f'f''' - ff^{iv}\right) + \left(3\alpha_1 + 2\alpha_2\right)f''^2 + 6\beta \mathrm{Re} f''' f''^2 - P_m f' - Frf'^2 + Hme^{-\delta\eta} + \lambda(\theta - N_r\phi - R_b\chi) = 0,$$
$$\left(1 + \frac{4}{3}R\,d\right)\theta'' + \mathrm{Pr} f\theta' - \mathrm{Pr}S_1 f' - \mathrm{Pr}\Gamma_1\left[f'^2\theta + S_1 f'^2 - ff'\theta' - ff''\theta - S_1 ff'' + f^2\theta''\right] + \mathrm{Pr}Hg\theta + \mathrm{Pr}Nb\,\theta'\phi\prime + \mathrm{Pr}Nt\theta'^2 = 0, \tag{9}$$
$$\phi'' + Lef\phi\prime - LeS_2 f' - Le\Gamma_2\left[f'^2\phi + S_2 f'^2 - ff'\phi\prime - ff''\phi - S_2 ff'' + f^2\phi''\right] + \frac{Nt}{Nb}\theta'' - LeCr\phi = 0,$$
$$\chi'' + L_b\left[f\chi\prime - f'\chi\right] - L_b S_3 f' - P_e\left[\phi''(\chi + \Omega) + \phi\prime\chi\prime\right] = 0.$$

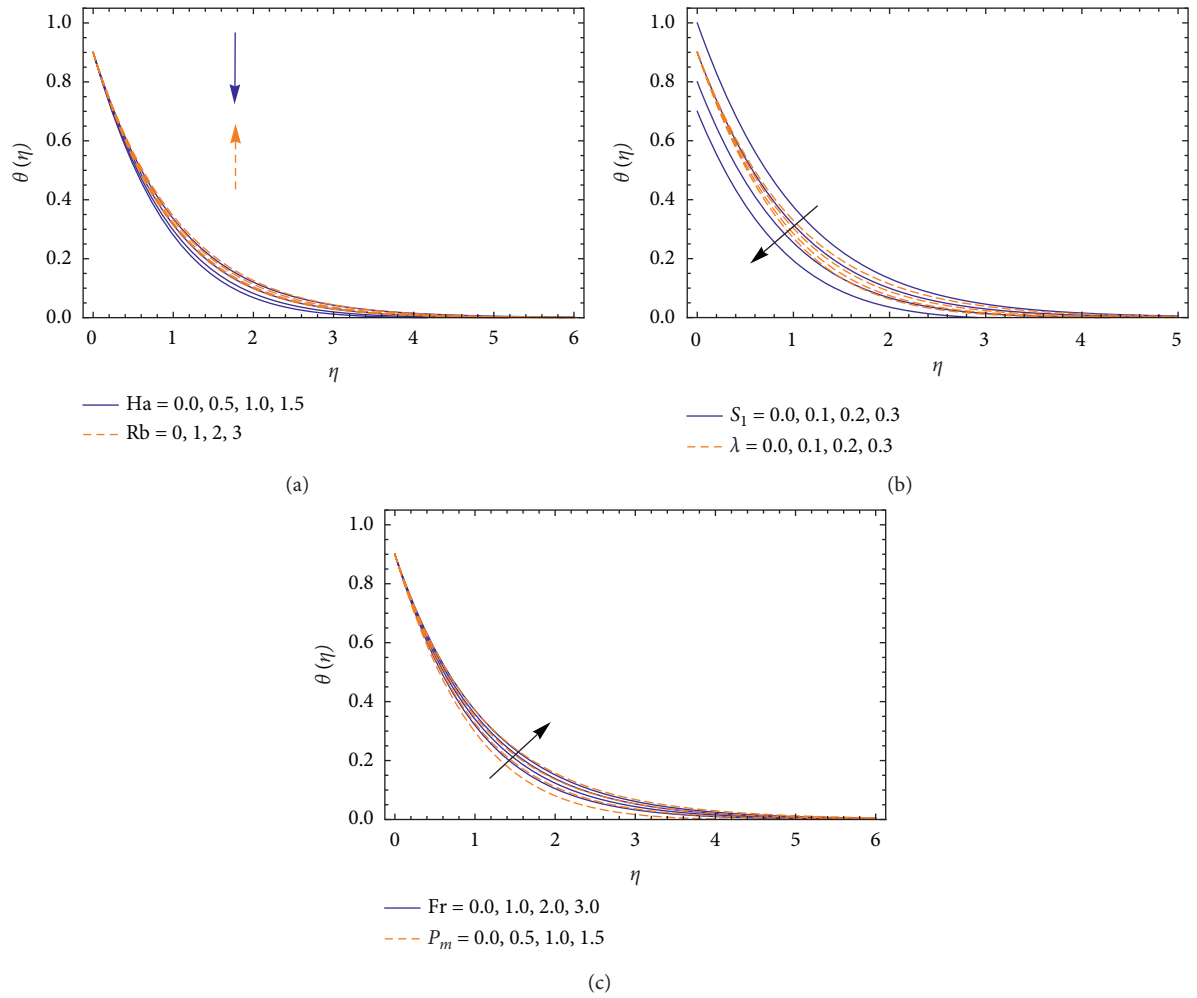

Figure 3: Temperature profile for different values of Ha, Rb, S_1, λ, Fr, and P_m.

The boundary conditions are specified in the following manner:

$$\begin{aligned} f(0) &= 0, \\ f'(0) &= 1, \\ \theta(0) &= 1 - S_1, \\ \phi(0) &= 1 - S_2, \\ \chi(0) &= 1 - S_3, \\ f'(\infty) &= 0, \\ \theta(\infty) &= 0, \\ \phi(\infty) &= 0, \\ \chi(\infty) &= 0, \end{aligned} \tag{10}$$

The nondimensional variables are

$$\text{Materiel parameters} = \left(\alpha_1 = \frac{aA_1^*}{\nu}, \alpha_2 = \frac{aA_2^*}{\nu}, \beta = \frac{a\beta_1^*}{\nu}\right),$$

$$\text{Reynolds number (Re)} = \frac{u_w x}{\nu},$$

$$\text{Porous medium } (P_m) = \frac{\nu}{k_p a},$$

$$\text{Forchheimer number } (Fr) = \frac{C_b}{\sqrt{k_p}},$$

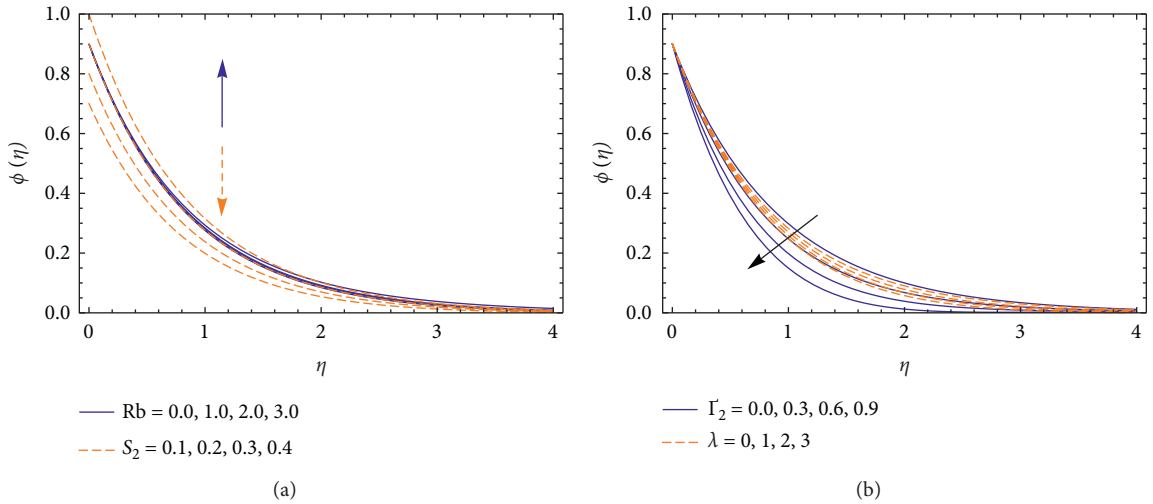

Figure 4: Nanoparticle concentration profile for different values of Ha, Rb, S_1, λ, Fr, and P_m.

$$
\begin{aligned}
\text{Prandtl number}\,(\text{Pr}) &= \frac{\rho C_p}{k},\\
\text{Radiation parameter}\,(Rd) &= \frac{\left(4\sigma^* T_\infty^3\right)}{\left(kk^*\right)},\\
\text{Heat generation parameter}\,(Hg) &= \frac{Q_0}{\rho c_p},\\
\text{Heat thermal relaxation parameter}\,(\Gamma_1) &= \lambda_T a,\\
\text{Mass thermal relaxation parameter}\,(\Gamma_2) &= \lambda_C a,\\
\text{Mixed convection parameter}\,(\lambda) &= \frac{\beta\gamma\left(1-C_\infty\right)\left(T_w-T_0\right)}{au_w},\\
\text{Buoyancy ratio parameter}\,(N_r) &= \frac{\left(\rho_p-\rho_f\right)}{\beta\rho_f}\frac{\left(C_w-C_0\right)}{\left(\hat{T}_w-\hat{T}_0\right)},\\
\text{Bioconvection Rayleigh number}\,(R_b) &= \frac{\gamma\left(N_w-N_0\right)\left(\rho_m-\rho_f\right)}{\beta\rho_f\left(1-C_\infty\right)\left(T_w-T_0\right)},\\
\text{Thermophoresis parameter}\,(N_t) &= \frac{\tau D_T\left(T_w-T_0\right)}{\upsilon},\\
\text{Brownian motion parameter}\,(N_b) &= \frac{\tau D_B\left(C_w-C_0\right)}{\nu},\\
\text{Lewis number}\,(Le) &= \frac{\nu}{D_B},\\
\text{Bioconvection Lewis number}\,(L_b) &= \frac{\nu}{D_m},\\
\text{Bioconvection Peclet number}\,(P_e) &= \frac{bW_c}{D_m},\\
\text{Microorganisms concentration difference parameter}\,(\Omega) &= \frac{N_\infty}{N_w-N_0},\\
\text{Thermal stratification parameter}\,(S_1) &= \frac{b_2}{b_1},\\
\text{Mass stratification parameter}\,(S_2) &= \frac{d_2}{d_1},\\
\text{Motile density stratification parameter}\,(S_3) &= \frac{e_2}{e_1}.
\end{aligned}
\tag{11}
$$

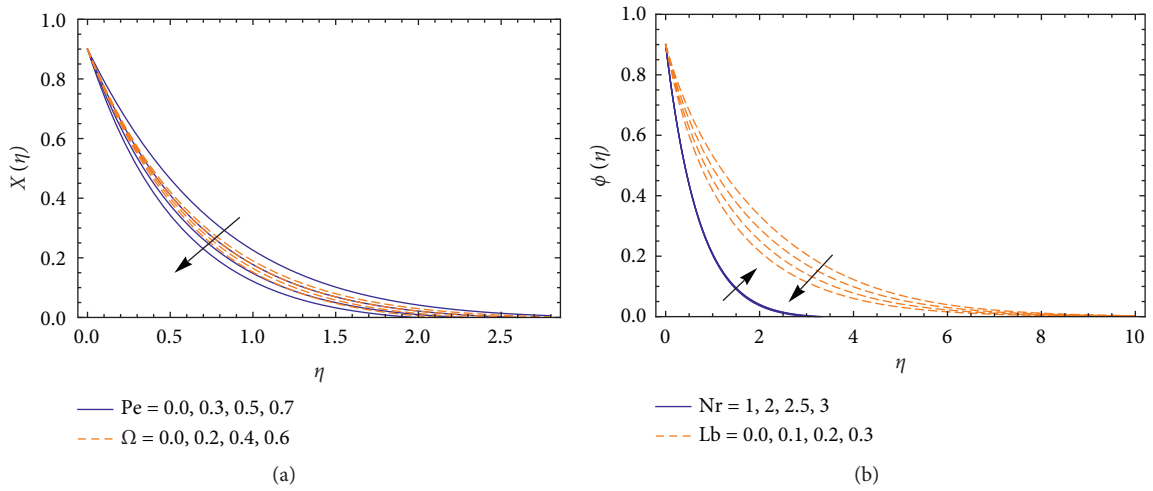

Figure 5: Microorganism profile for different values of P_e, Ω, Nr, and L_b.

Application of physical entitles are

$$\begin{aligned} C_f \mathrm{Re}^{-0.5} &= f''(0) + \alpha_1 f'(0) f'''(0) + \beta \mathrm{Re}[f''(0)]^3, \\ Nu_x \mathrm{Re}^{-0.5} &= -\left(1 + \frac{4}{3}\mathrm{Rd}\right)\theta'(0), \\ Sh_x \mathrm{Re}^{-0.5} &= -\phi\prime(0), \\ Nn_x \mathrm{Re}^{-0.5} &= -\chi\prime(0). \end{aligned} \tag{12}$$

3. Modelling of Entropy Generation

For the third grade nanoliquid, the entropy generation rate is as follows:

$$\begin{aligned} S''_{\mathrm{gen}} = \left\langle \frac{K_1}{T_\infty^2}\left[\left(\frac{\partial T}{\partial x}\right)^2 + \left(\frac{\partial T}{\partial y}\right)^2 + \frac{16\sigma^* T_\infty^3}{3kk^*}\left(\frac{\partial T}{\partial y}\right)^2\right] + \frac{\mu}{T_\infty}\left[2\left(\frac{\partial u}{\partial x}\right)^2 + \left(\frac{\partial v}{\partial y}\right)^2\right] + \left[\frac{\partial u}{\partial y} + \frac{\partial v}{\partial x}\right]^2 + \frac{RD}{C_\infty}\left[\left(\frac{\partial C}{\partial x}\right)^2 + \left(\frac{\partial C}{\partial y}\right)^2\right] \\ + \frac{RD}{T_\infty}\left[\left(\frac{\partial T}{\partial x}\right)\left(\frac{\partial C}{\partial x}\right) + \left(\frac{\partial T}{\partial y}\right)\left(\frac{\partial C}{\partial y}\right)\right] + \frac{RD}{N_\infty}\left(\frac{\partial N}{\partial y}\right)^2 + \frac{RD}{T_\infty}\left[\left(\frac{\partial T}{\partial x}\right)\left(\frac{\partial N}{\partial x}\right) + \left(\frac{\partial T}{\partial y}\right)\left(\frac{\partial N}{\partial y}\right)\right]\right\rangle, \end{aligned} \tag{13}$$

Equation (13) was changed by using the boundary layer approximation.

$$\begin{aligned} S'''_{\mathrm{gen}} &= \left\langle \frac{K_1}{T_\infty^2}\left[\left(\frac{\partial T}{\partial y}\right)^2 + \frac{16\sigma^* T_\infty^3}{3kk^*}\left(\frac{\partial T}{\partial y}\right)^2\right] + \frac{\mu}{T_\infty}\left(\frac{\partial u}{\partial y}\right)^2 + \frac{RD}{C_\infty}\left(\frac{\partial C}{\partial y}\right)^2 + \frac{RD}{T_\infty}\left(\frac{\partial T}{\partial y}\right)\left(\frac{\partial C}{\partial y}\right) + \frac{RD}{N_\infty}\left(\frac{\partial N}{\partial y}\right)^2 + \frac{RD}{T_\infty}\left[\left(\frac{\partial T}{\partial y}\right)\left(\frac{\partial N}{\partial y}\right)\right]\right\rangle, \\ N_T &= \frac{K_1}{T_\infty^2}\left[\left(\frac{\partial T}{\partial y}\right)^2 + \frac{16\sigma^* T_\infty^3}{3kk^*}\left(\frac{\partial T}{\partial y}\right)^2\right] = \text{“Entropy contribution due to heat transmission”}, \\ N_f &= \frac{\mu}{T_\infty}\left(\frac{\partial u}{\partial y}\right)^2 = \text{“Entropy contribution due to fluid friction”}, \\ N_C &= \frac{RD}{C_\infty}\left(\frac{\partial C}{\partial y}\right)^2 + \frac{RD}{T_\infty}\left(\frac{\partial T}{\partial y}\right)\left(\frac{\partial C}{\partial y}\right) = \text{“Entropy contribution due to mass transmission”}, \\ S'''_{\mathrm{gen}} &= N_T + N_f + N_C + N_m. \end{aligned} \tag{14}$$

The typical entropy generation rate S'''_0 is given by

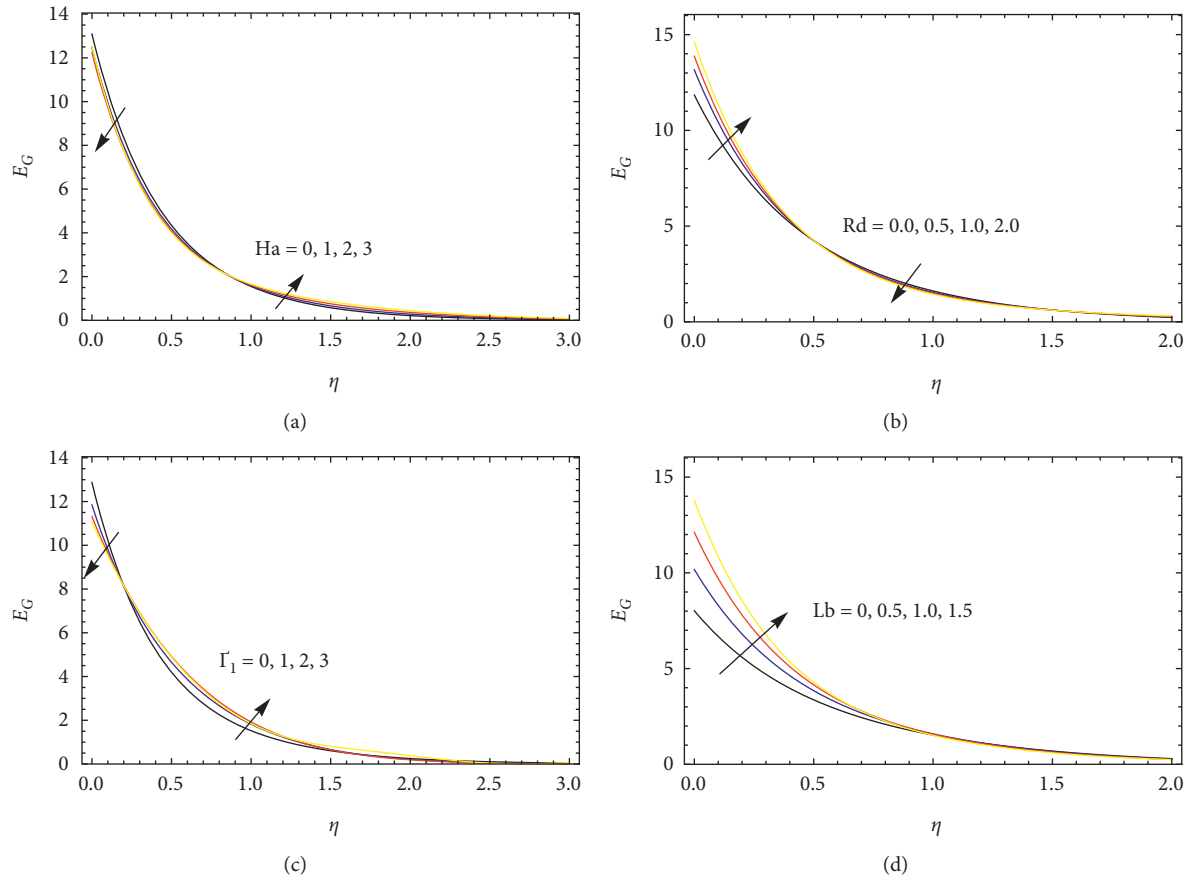

Figure 6: Entropy generation profile for different values of Ha, Rd, Γ_1, and Lb.

$$S_0''' = \left\langle \frac{K_1}{T_\infty^2} \frac{(\Delta T)^2}{l^2} \right\rangle. \tag{15}$$

As a consequence, the dimensionless entropy generation number may be calculated by using the following formula:

$$E_G = \frac{S_{\text{gen}}'''}{S_0'''}. \tag{16}$$

As a result, the total entropy generation number has the corresponding dimensionless form:

$$E_G = \text{Re}\left(1 + \frac{4}{3}Rd\right)\theta'^2 + \text{Re}\frac{Br}{\Omega}f''^2 + \text{Re}\left(\frac{\zeta}{\Omega}\right)^2 \lambda\phi'^2 + \text{Re}\frac{\zeta}{\Omega}\lambda\phi\prime\theta' + \text{Re}\lambda\left(\frac{\zeta}{\Pi}\right)^2 \chi\prime + \text{Re}\lambda\left(\frac{\zeta}{\Pi}\right)\chi\prime\theta'. \tag{17}$$

Expression of the Bejan number is

$$Be = \frac{N_T + N_C + N_m}{E_G}. \tag{18}$$

4. Homotopy Solutions

The governing equations are solved analytically by applying the HAM scheme [18, 22–32]. In this regard, initially, we fix the initial approximation

$$\begin{aligned} f_0(\eta) &= [1 - e^{-\eta}], \\ \theta_0(\eta) &= [(1 - S_1)e^{-\eta}], \\ \phi_0(\eta) &= [(1 - S_2)e^{-\eta}], \\ \chi_0(\eta) &= [(1 - S_3)e^{-\eta}]. \end{aligned} \tag{19}$$

The linear operator is

$$\begin{aligned} \hat{L}_f &= \frac{\hat{\mathrm{d}}^3 f}{\mathrm{d}\eta^3} - \frac{\mathrm{d}f}{\mathrm{d}\eta}, \\ \hat{L}_\theta &= \frac{\hat{\mathrm{d}}^2 \theta}{\mathrm{d}\eta^2} - \theta, \\ \hat{L}_\phi &= \frac{\hat{\mathrm{d}}^2 \phi}{\mathrm{d}\eta^2} - \phi, \\ \hat{L}_\chi &= \frac{\hat{\mathrm{d}}^2 \chi}{\mathrm{d}\eta^2} - \chi, \end{aligned} \tag{20}$$

with the property

$$\begin{aligned} \hat{L}_f[\Psi_1 + \Psi_2 e^{\eta} + \Psi_3 e^{-\eta}] &= 0, \\ \hat{L}_\theta[\Psi_4 e^{\eta} + \Psi_5 e^{-\eta}] &= 0, \\ \hat{L}_\phi[\Psi_6 e^{\eta} + \Psi_7 e^{-\eta}] &= 0, \\ \hat{L}_\chi[\Psi_8 e^{\eta} + \Psi_9 e^{-\eta}] &= 0. \end{aligned} \tag{21}$$

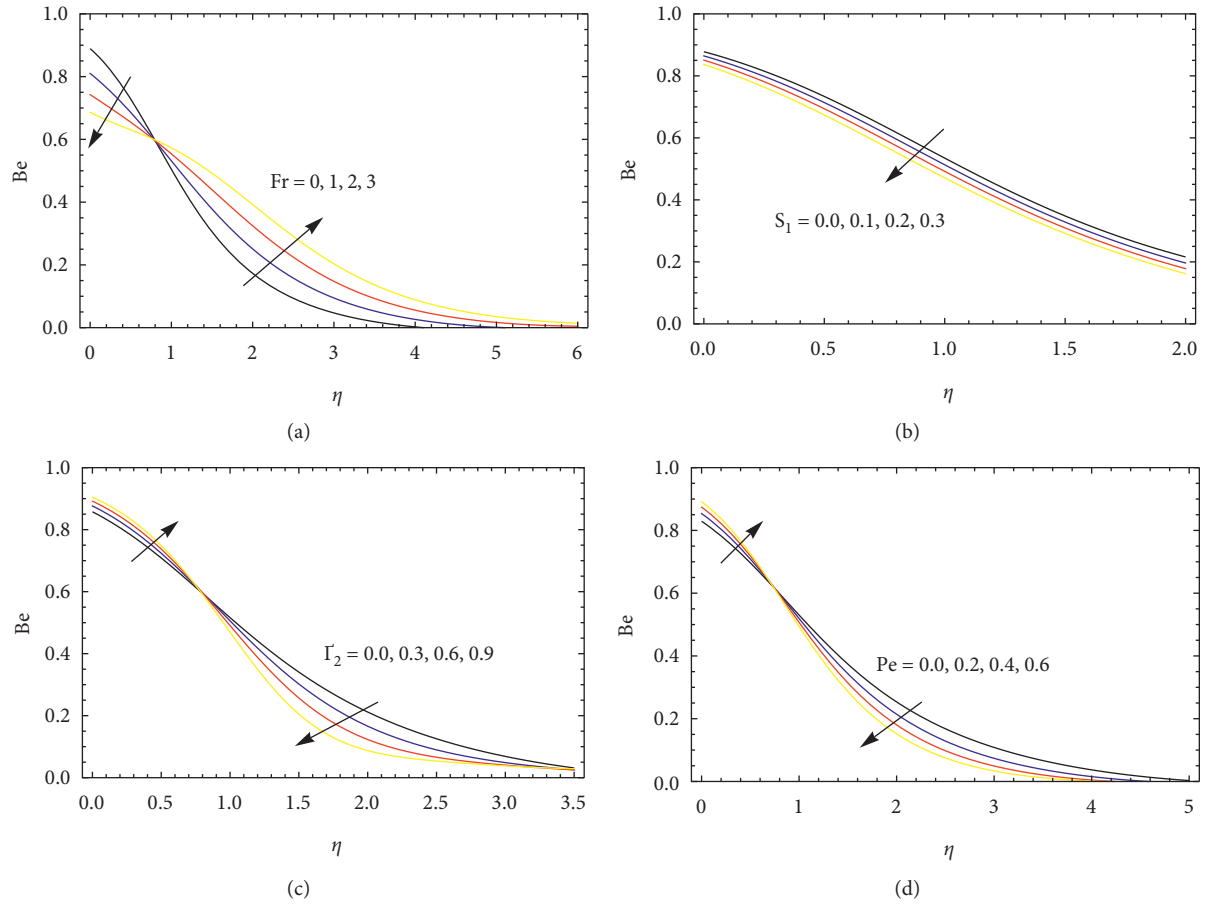

Figure 7: Bejan number profile for different values of Fr, S_1, Γ_2, and Pe.

Here, $\Psi_i [i = 1 - 9]$ are the arbitrary constants.

After utilizing the jth order HAM, we get

$$\begin{aligned} f_j(\eta) &= f_j^*(\eta) + \Psi_1 + \Psi_2 e^{\eta} + \Psi_3 e^{-\eta}, \\ \theta_j(\eta) &= \theta_j^*(\eta) + \Psi_4 e^{\eta} + \Psi_5 e^{-\eta}, \\ \phi_j(\eta) &= \phi_j^*(\eta) + \Psi_6 e^{\eta} + \Psi_7 e^{-\eta}, \\ \chi_j(\eta) &= \chi_j^*(\eta) + \Psi_8 e^{\eta} + \Psi_9 e^{-\eta}. \end{aligned} \tag{22}$$

Here, $f_j^*(\eta), \theta_j^*(\eta), \phi_j^*(\eta)$, and $\chi_j^*(\eta)$ are the particular solutions.

The HAM includes the auxiliary parameters $(h_f, h_\theta, h_\phi$, and $h_\chi)$, and these are the responsible for solution convergence.

5. Convergence Analysis

The convergence values are of h_f, h_θ, h_ϕ, and h_χ, are plotted in Figure 1. The range of convergence is $-0.4 \le h_f \le -0.1$, $-0.5 \le h_\theta, h_\phi \le -0.1$, $-0.5 \le h_\phi \le 0.0$, and $-0.55 \le h_\chi \le -0.2$. Table 1 observes $f''(0)$, $\theta'(0)$, $\phi\prime(0)$, and $\chi\prime(0)$ for the $15th$ order of estimation. The convergence range of the current solution is $h_f = 0.35$ and $h_\theta = h_\phi = h_\chi = -0.30$.

6. Results and Discussion

This section focused on the effects of divergent physical factors on fluid velocity, fluid temperature, nanoparticle volume fraction, motile microbe density, skin friction coefficients, local Nusselt number, and local Sherwood number. Table 1 provides the validation of the present analysis with previously published results [18, 22]. From this comparison, we found that the current computation is an optimum one.

In this section, we focused on the variations of fluid velocity, fluid temperature, nanoparticle volume fraction, motile microorganism density, skin friction coefficients, local Nusselt number, and local Sherwood number for divergent physical parameters. Figures 2(a)–2(d)) provide the impact of $\alpha_1, \alpha_2, Ha, P_m, P_e, N_r, R_b$, and S_1 on the velocity profile. It is detected that the fluid velocity enriches when escalating the quantity of α_1, α_2, Ha, and P_e, and it downfalls when enhancing the quantity of P_m, N_r, R_b, and S_1. Physically, the modified Hartmann number leads to strengthening the external electric field, and this causes to increase the fluid velocity. The temperature variations of $Ha, R_b, S_1, \lambda, Fr$, and P_m are presented in Figures 3(a)–3(c)). It is seen that the fluid temperature escalates when raising the quantity of R_b, Fr, and P_m, and the opposite behaviour was attained when varying the values of Ha, S_1, and λ. Figures 4(a) and

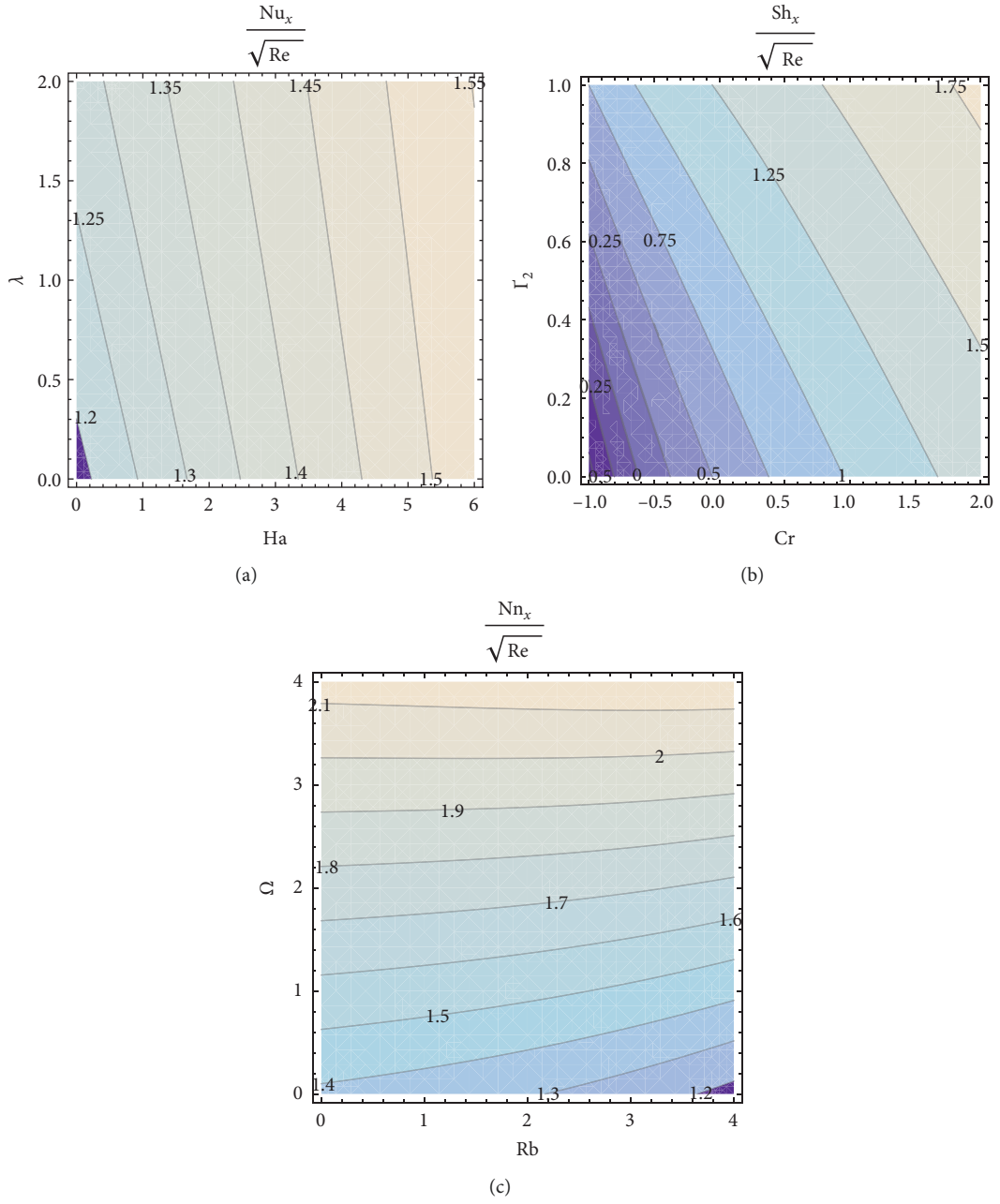

FIGURE 8: (a) "Nusselt number" for Ha and λ, (b) "Sherwood number" for Γ_2 and Cr, and (c) "Microorganism density number" for Ω and Rb.

4(b)) portray the consequences of R_b, S_2, Γ_2, and λ on the concentration profile. It is concluded that the fluid concentration increases when rising the quantity of R_b, and it reduces when strengthening the values of S_2, Γ_2, and λ. The microorganism profile for various values of P_e, Ω, Nr, and L_b is illustrated in Figures 5(a) and 5(b) and found that the microorganism profile suppresses when enhancing the P_e, Ω, and L_b quantities, and it escalates when escalating the values of Nr.

Figures 6(a)–6(d) display the consequences of Ha, Rd, Γ_1, and Lb on the entropy generation profile. It is seen that the entropy generation diminishes near the plate and upturns away from the plate for varying the Ha and Γ_1 values, and the opposite behavior occurs for enhancing the Rd values. In addition, the Lb leads to enrich the entropy generation. The changes of the Bejan number for different values of Fr, S_1, Γ_2, and Pe are presented in Figures 7(a)–7(d) and seen that the Bejan number upturns near the plate and downfalls away from the plate for changing the Γ_2 and s values. The quite opposite trend attains for varying the Fr values. The S_1 values lead to reduce the Bejan number.

Fig. 8(a) reveals the collective effect of Ha and λ on [Nu]_x with other parameters are kept fixed heat transfer rate [Nu]_x is abridged with growing amounts of both Ha and λ. Figure 8(b) explores the graphical assessment of Sherwood number Sh_x against the variations in Cr and Γ_2 with other parameters are retained fixed. The Sherwood number Sh_x is improved with the enhancement in Cr and Γ_2. Figure 8(c)

Table. 1: Comparison of $C_f Re^{-0.5}$ for the limiting conditions. $P_m = Fr = Hm = \lambda = N_r = R_b = 0$.

α_1	α_2	β	Re	Imtiaz et al. [22]	Loganathan et al. [18]	Present
0.0	0.1	0.1	0.1	0.04605	0.04605	0.04605
0.1				1.06680	1.06680	1.06680
0.2				1.17470	1.17470	1.17470
	0.0	0.1	0.1	1.12010	1.12010	1.12010
0.1	0.1			1.06680	1.06680	1.06680
	0.2			1.01830	1.01830	1.01830
	0.1	0.0		1.06290	1.06290	1.06290
		0.1		1.06680	1.06680	1.06680
		0.2		1.07030	1.07030	1.07030
0.1		0.1	0.0	1.06290	1.06290	1.06290
			0.1	1.06680	1.06680	1.06680
			0.2	1.07060	1.07060	1.07060

describes the graphical evaluation of the microorganism density number Nn_x against the variations in Rb and Ω with other parameters as taken fixed. The microorganism density number Nn_x is improved with the enhancement in Rb and Ω.

7. Conclusions

In this article, we analyse the performance of heat-mass effects of third grade nanofluid flow through a triply stratified medium with swimming of nanoparticles, and gyrostatic microorganisms are swum into this flow. The non-Fourier heat and mass flux's theory were used to frame the energy and nanoparticle concentration equations. The reduced models were analytically solved by applying the HAM scheme. The major outcomes are summarized as follows:

(i) The fluid velocity enhances when raising the modified Hartmann number, and it suppresses for a larger quantity of the thermal relaxation parameter.

(ii) The fluid temperature rises when enhancing the Forchheimer number and downfalls when increasing the bioconvection parameter.

(iii) The fluid concentration decays when strengthening the solutal relaxation time and stratification parameters.

(iv) The microorganism profile reduces when improving the quantity of P_e, Ω, and L_b, and it escalates when escalating the values of Nr.

(v) The entropy rate is enhanced for higher values of the heat thermal relaxation parameter and bioconvection Lewis number.

(vi) The Bejan number diminishes for the solutal thermal relaxation parameter, thermal stratification, and bioconvection Peclet number.

Data Availability

"The raw data supporting the conclusion of this report will be made available by the corresponding author without undue reservation."

Conflicts of Interest

The author declares that there are no conflicts of interest.

References

[1] S. U. S. Choi, "Enhancing thermal conductivity of fluids with nanoparticles," *Proceedings of the ASME International Mechanical Engineering Congress and Exposition*, vol. 66, pp. 99–105, 1995.

[2] W. A. Khan and I. Pop, "Boundary-layer flow of a nanofluid past a stretching sheet," *International Journal of Heat and Mass Transfer*, vol. 53, no. 11-12, pp. 2477–2483, 2010.

[3] P. Barnoon and D. Toghraie, "Numerical investigation of laminar flow and heat transfer of non-Newtonian nanofluid within a porous medium," *Powder Technology*, vol. 325, pp. 78–91, 2018.

[4] M. Ghalambaz, A. Noghrehabadi, and A. Ghanbarzadeh, "Natural convection of nanofluids over a convectively heated vertical plate embedded in a porous medium," *Brazilian Journal of Chemical Engineering*, vol. 31, no. 2, pp. 413–427, 2014.

[5] A. Aziz and W. A. Khan, "Natural convective boundary layer flow of a nanofluid past a convectively heated vertical plate," *International Journal of Thermal Sciences*, vol. 52, pp. 83–90, 2012.

[6] R. Ahmad, M. Mustafa, and S. Hina, "Buongiornos model for fluid flow around a moving thin needle in a flowing nanofluid: a numerical study," *Chinese Journal of Physics*, vol. 55, no. 4, pp. 1264–1274, 2017.

[7] B. C. Prasannakumara, M. R. Krishnamurthy, B. J. Gireesha, and R. S. R. Gorla, "Effect of multiple slips and thermal radiation on MHD flow of Jeffery nanofluid with heat transfer," *Journal of Nanofluids*, vol. 5, no. 1, pp. 82–93, 2016.

[8] H. Waqas, A. Kafait, T. Muhammad, and U. Farooq, "Numerical study for bio-convection flow of tangent hyperbolic nanofluid over a Riga plate with activation energy," *Alexandria Engineering Journal*, vol. 61, no. 2, pp. 1803–1814, 2022.

[9] M. J. Uddin, Y. Alginahi, O. A. Bég, and M. Kabir, "Numerical solutions for gyrotactic bioconvection in nanofluid-saturated porous media with Stefan blowing and multiple slip effects," *Computers & Mathematics with Applications*, vol. 72, no. 10, pp. 2562–2581, 2016.

[10] A. S. Alshomrani, M. Z. Ullah, and D. Baleanu, "Importance of multiple slips on bioconvection flow of cross nanofluid past a wedge with gyrotactic motile microorganisms," *Case Studies in Thermal Engineering*, vol. 22, Article ID 100798, 2020.

[11] T. Muhammad, S. Z. Alamri, H. Waqas, D. Habib, and R. Ellahi, "Bioconvection flow of magnetized Carreau nanofluid under the influence of slip over a wedge with motile microorganisms," *Journal of Thermal Analysis and Calorimetry*, vol. 143, no. 2, pp. 945–957, 2021.

[12] J. Fourier, "Theorie analytique de la chaleur, par M," *Fourier, Chez Firmin Didot, pre et fils*, 1822.
[13] C. Cattaneo, "Sulla conduzione del calore," *Proceedings of the Mathematical and Physical Seminar of the University of Modena and Reggio Emilia*, vol. 3, Article ID 83101, 1948.
[14] C. J. Christov, "On frame indifferent formulation of the maxwell-Cattaneo model of finite speed heat conduction," *Mechanics Research Communications*, vol. 36, no. 4, pp. 481–486, 2009.
[15] T. Salahuddin, M. Awais, M. Khan, and M. Altanji, "Analysis of transport phenomenon in cross fluid using Cattaneo-Christov theory for heat and mass fluxes with variable viscosity," *International Communications in Heat and Mass Transfer*, vol. 129, Article ID 105664, 2021.
[16] U. Farooq, H. Waqas, M. Imran, A. Albakri, and T. Muhammad, "Numerical investigation for melting heat transport of nanofluids due to stretching surface with Cattaneo-Christov thermal model," *Alexandria Engineering Journal*, vol. 61, no. 9, pp. 6635–6644, 2022.
[17] H. Waqas, T. Muhammad, S. Noreen, U. Farooq, and M. Alghamdi, "Cattaneo-Christov heat flux and entropy generation on hybrid nanofluid flow in a nozzle of rocket engine with melting heat transfer," *Case Studies in Thermal Engineering*, vol. 28, Article ID 101504, 2021.
[18] K. Loganathan, K. Mohana, M. Mohanraj, P. Sakthivel, and S. Rajan, "Impact of third-grade nanofluid flow across a convective surface in the presence of inclined Lorentz force: an approach to entropy optimization," *Journal of Thermal Analysis and Calorimetry*, vol. 144, no. 5, pp. 1935–1947, 2020.
[19] R. S. Rivlin and J. Ericksen, "Stress-deformation relations for isotropic materials," *Collected Papers of RS Rivlin*, pp. 911–1013, Springer, Berlin, Germany, 1997.
[20] R. Fosdick and K. Rajagopal, Eds., *Proceedings of the Royal Society of London A: Mathematical, Physical and Engineering Sciences*The Royal Society, London, UK, 1980.
[21] M. Pakdemirli, "The boundary layer equations of third-grade fluids," *International Journal of Non-linear Mechanics*, vol. 27, no. 5, pp. 785–793, 1992.
[22] M. Imtiaz, A. Alsaedi, A. Shafiq, and T. Hayat, "Impact of chemical reaction on third grade fluid flow with Cattaneo-Christov heat flux," *Journal of Molecular Liquids*, vol. 229, pp. 501–507, 2017.
[23] T. Hayat, M. Ijaz Khan, S. Qayyum, and A. Alsaedi, "Modern developments about statis-tical declaration and probable error for skin friction and Nusselt number with copper and silver nanoparticles," *Chinese Journal of Physics*, vol. 55, no. 6, pp. 2501–2513, 2017.
[24] M. Farooq, M. Javed, M. Ijaz Khan, A. Anjum, and T. Hayat, "Melting heat transfer and double stratification in stagnation flow of viscous nanofluid," *Results in Physics*, vol. 7, pp. 2296–2301, 2017.
[25] M. Waqas, M. Farooq, M. I. Khan, A. Alsaedi, T. Hayat, and T. Yasmeen, "Magnetohydrodynamic (MHD) mixed convection flow of micropolar liquid due to nonlinear stretched sheet with convective condition," *International Journal of Heat and Mass Transfer*, vol. 102, pp. 766–772, 2016.
[26] K. Loganathan and S. Rajan, "An entropy approach of Williamson nanofluid flow with Joule heating and zero nanoparticle mass flux," *Journal of Thermal Analysis and Calorimetry*, vol. 141, no. 6, pp. 2599–2612, 2020.
[27] T. Hayat, F. Shah, M. I. Khan, and A. Alsaedi, "Framing the performance of heat absorption/generation and thermal radiation in chemically reactive Darcy–Forchheimer flow," *Results in Physics*, vol. 7, pp. 3390–3395, 2017.
[28] T. S. Karthik, K. Loganathan, A. N. Shankar et al., "Zero and nonzero mass flux effects of bioconvective viscoelastic nanofluid over a 3D Riga surface with the swimming of gyrotactic microorganisms," *Advances in Mathematical Physics*, vol. 2021, Article ID 9914134, 13 pages, 2021.
[29] I. Ahmad, M. Faisal, K. Loganathan, M. Z. Kiyani, and N. Namgyel, "Nonlinear mixed convective bidirectional dynamics of double stratified radiative Oldroyd-B nanofluid flow with heat source/sink and higher-order chemical reaction," *Mathematical Problems in Engineering*, vol. 2022, 16 pages, Article ID 9732083, 2022.
[30] S. Eswaramoorthi, K. Loganathan, R. Jain, and S. Gyeltshen, "Darcy-forchheimer 3D flow of glycerin-based carbon nanotubes on a Riga plate with nonlinear thermal radiation and cattaneo-christov heat flux," *Journal of Nanomaterials*, vol. 2022, Article ID 5286921, 20 pages, 2022.
[31] S. Eswaramoorthi, K. Loganathan, M. Faisal, T. Botmart, and N. A. Shah, "Analytical and numerical investigation of Darcy-Forchheimer flow of a nonlinear-radiative non-Newtonian fluid over a Riga plate with entropy optimization," *Ain Shams Engineering Journal*, Article ID 101887, 2022.
[32] K. Loganathan, N. Alessa, K. Tamilvanan, and F. S. Alshammari, "Significances of Darcy–Forchheimer porous medium in third-grade nanofluid flow with entropy features," *The European Physical Journal - Special Topics*, vol. 230, pp. 1293–1305, 2021.